Two-Dimensional Frank-Kasper *Z* Phase with One Unit-Cell Thickness

Xie Hongbo (xiehongbo@mail.neu.edu.cn)
Northeastern University, Shenyang
Junyuan Bai
Northeastern University
Haiyan Ren
Northeastern University, Shenyang
Shanshan Li
Northeastern University
Hucheng Pan
Northeastern University
Yuping Ren
Northeastern University
Gaowu Qin
Northeastern University https://orcid.org/0000-0002-0852-6715

Article

Keywords: Z phase, Frank-Kasper phases, condensed matter

Posted Date: December 16th, 2020

DOI: https://doi.org/10.21203/rs.3.rs-123163/v1

Abstract

Z phase is one of the three basic units by which the Frank-Kasper phases are generally assembled. Compared to the other two basic units, i.e., A15 and C15 structures, the Z phase structure is rarely experimentally observed because of a relatively large volume ratio among the constituents to inhibit its formation. Moreover, the discovered Z structures are generally the three-dimensional (3D) ordered Gibbs bulk phases to conform to their thermodynamic stability. Herein, we confirmed the existence of a metastable two-dimensional (2D) Frank-Kasper Z phase with one unit-cell height in the crystallography in a model Mg-Sm-Zn system, by using aberration-corrected high-angle annular dark-field scanning transmission electron microscopy (HAADF-STEM) combined with density functional theory (DFT) calculations. This finding is important for understanding the relationship between the traditional crystal structures and the quasicrystals, and it is also expected to provide a new insight to understand the clustering and stacking behavior of atoms in condensed matters.

Main Text

Frank-Kasper phase is a class of ordered crystals composed of the topologically close-packed atomic-layers [1, 2], in which the atoms with a smaller radius form as the close-packed planes and the atoms with a larger radius embed in the tetrahedral gaps. So far, there have 28 different types of Frank-Kasper phases found experimentally (in Supplemental Table S1), including in metal alloys [3, 4], inorganic colloids [5, 6], and soft matters [7-10].

Generally, the Frank-Kasper phases can be considered as ordered approximates of quasi-periodic crystals due to some shared construction rules from atomic clustering and stacking [11]. Since the Al-Mn icosahedral quasicrystal discovered in 1984 by *Shechtman et al* [12], the complex architectures of Frank-Kasper phases are considered as a link between the traditional simple periodic structures (such as the face-centered cubic, hexagonal close-packed, and body-centered cubic structures) and quasicrystals [10, 13].

From the viewpoint of crystallography characteristics, there are two types of Frank-Kasper structures which be constructed by three basic units of A_{15} (representative alloy: Cr_3Si), C_{15} (representative alloy: $MgCu_2$), and Z (representative alloy: Zr_4Al_3) fundamental structures frequently observed to date, *i.e.*, the pentagonal Frank-Kasper phases and the hexagonal Frank-Kasper phases [14, 15]. The pentagonal Frank-Kasper structure (see Supplemental Figure S1) can be considered as a periodic arrangement of icosahedron (coordination number (*CN*) = 12) columns along the pseudo 10-fold axis promoting the formation of C_{15} (parallelogram) and *Z* (rectangle) plane tiling patterns, and the parallelogram and rectangular patterns self-assemble under some geometrical constraints to generate the present pentagonal phases. Similarly, the hexagonal Frank-Kasper phases (see Supplemental Figure S2) can be regarded as a structure formed by the icositetrahedron (*CN* = 14) columns arranged periodically along the pseudo 12-fold axis, to build square A_{15} and rhombic *Z* plane tiling patterns, and the bonding of the two patterns leads to the generation of the hexagonal phases.

To better understand the relationship between these Frank-Kasper structures, Fig. 1 provides a relationship between the average *CN* and the fraction of *CN* = 15 polyhedra in a Frank-Kasper phase, and all these 28 types of Frank-Kasper phases are located in a triangle with the three basic Frank-Kasper structures located at three vertices. In which the *pentagonal* Frank-Kasper phases assembled by the C_{15} and *Z* plane tiling patterns are represented by the red balls; the *hexagonal* Frank-Kasper phases assembled by the A_{15} and *Z* plane tiling patterns are represented by the blue balls. The Z phase structure, the basic unit of both the pentagonal phases and the hexagonal phases, is represented by a ball with red and blue colors. We defined here the three fundamental structures of A_{15}, C_{15}, and Z phases as the first-order Frank-Kasper phases, and the complex phases assembled by any of three basic units as the second-order Frank-Kasper phases. And it can be found that the Z phase is the most important since it is the basic unit for assembling any of the second-order Frank-Kasper phases.

At present, the C_{15} fundamental Laves structure with a chemical formula of AB_2 and the A_{15} fundamental structure with a chemical formula of A_3B are found abundantly in metal alloys, and there are more than 900 kinds of Laves phases have been identified experimentally [3], and the high-temperature superconductors with A_{15} structure (such as Nb_3B, Nb_3Si, and Nb_3Ge) also exist extensively. However, the *Z* phase structure with a A_4B_3 chemical formula postulated by *Frank* & *Kasper* in 1959 are rarely observed to date [2]. Since a Zr_4Al_3 phase was proposed firstly by *C. G. Wilson et al.* in 1960 [16], this structure has not been confirmed by any other direct experimental observations to date except a recent report in soft matter [10]. And these two Z phases in both alloy and soft matter are three-dimensional blocks to maintain their thermodynamical stability.

In contrast, we reported here a new structured 2D Frank-Kasper *Z* phase in an aged Mg-Sm-Zn model system. More interestingly, the 2D Frank-Kasper *Z* precipitate with only one unit-cell height in the $_Z$ axis, and it is thermodynamically metastable. This finding would pave a way for understanding the formation mechanism of the second-order Frank-Kasper phases and quasicrystals in general condensed matters.

A Mg-4Sm-2Sm (in wt.%) alloy was induction-melted and solution-treated at 520 °C for 12 h, followed by aging at 200 °C for 48 h (the experimental details are in the Supplemental Materials). The HAADF-STEM images of the aged-sample, viewed along the $_{a}$, $_{a}$, and $_{a}$ directions, are shown in Fig. 2. Low-magnification HAADF-STEM images (Figs. 2a-c) show that there are high-density nanosized precipitate-plates distributed in the *α*-Mg grains, whose length is approximately 30~50 nm, with a height less than 1 nm lying on the $\{0001\}_{\alpha}$ basal planes. Bright-filed images and corresponding select-area electron diffraction (SAED) patterns are provided in Supplemental Figure S3. This precipitate has been named by γ" phase in the field of magnesium alloys, but its fine structure has not been well documented [17-19].

To precisely reveal the crystal structure and atomic coordinates of the precipitate-plates, atomic imaging by HAADF-STEM was used. Atomic-scale HAADF-STEM image of the precipitate-nanoplates in Fig. 2a, is enlarged and shown in Fig. 2d. The $_{a}$ enlarged image shows that there are many bright dots inside the precipitate-nanoplate, and each bright dot represents a Sm-rich atomic column because the brightness of

individual atomic column in HAADF-STEM image approximates the square of the average atomic numbers (the atom number is 12 for Mg, 30 for Zn, and 62 for Sm) [20, 21]. The Sm-enriched atomic columns distribute along the < >$_{\alpha}$ directions and are separated by a constatnt distance. It can thus be concluded that the precipitate-nanoplate with an ordered hexagonal structure, and the corresponding lattice image is highlighted by a red 60° rhombus in the top-right inset in Fig. 2d. The crystal lattice constant of *a* can also be measured to be ~5.56 Å.

Local part of the precipitate-nanoplates in Fig. 2b is further enlarged and shown in Fig. 2e. The $_{a}$ enlarged image shows that the brightest dots located in the sub-outer layer correspond to the Sm atomic columns and the bright dots distributing on the central layer correspond to the Zn atomic columns with the help of the Z-contrast of Sm and Zn, which are represented by the blue and yellow circles in Fig. 2e, respectively. As a result, the precipitate-nanoplate is consisted of five atomic layers, i.e., the Mg / Sm / Zn / Sm / Mg atomic stacking structure, as displayed in the inset of Fig. 2e. And the atomic inter-distances of $h_{\text{Sm-Sm}}$ and $h_{\text{Mg-Mg}}$ can be measured to be ~ 3.49 Å and ~ 4.83 Å, respectively.

More evidences can be found from the HAADF-STEM image, detected along the $_{a}$ direction (Fig. 2f). The Zn atomic columns, as marked as the yellow solid-circles, always locate in the middle of four neighboring Sm atomic columns, and the Zn-dots wih weaker contrast can also be detected and hide between the two brighter contrast Sm atomic columns, as indicated in the yellow dashed-circles in inset of Fig. 2f. The results above indicate that the central-layer Zn atoms has a new grid structure that incoherent with $(0001)_{a}$ atomic layer.

Based on the atomic-scale HAADF-STEM results mentioned above, a new structured 2D Frank-Kasper *Z* phase model for the precipitate-nanoplate can be constructed. Modeled atomic arrangements and clusters of the 2D Frank-Kasper *Z* phase are displayed in Fig. 3, in which the Mg, Sm and Zn atoms are presented by the red, blue, and yellow spheres, respectively. And the structural information of the Frank-Kasper *Z* phase, as well as the atomic coordinates are presented in Supplemental Table S2. The most unique features of the Frank-Kasper *Z* phase, *i.e.*, the rhombic tiling units (blue rhombic) formed by a periodic arrangement of the icositetrahedron clusters (cyan circle) in the $_{Z}$ axis, and the rectangle tiling units (red rectangle) generated by a periodic arrangement of the icosahedron columns (yellow circle) along the $_{Z}$ direction, can be observed clearly in Figs. 3a and 3b. The two outmost layers correspond to the Mg atoms, and the distance between adjacent Mg atoms is ~ 3.21 Å. Moreover, one Mg atom is surrounded by three equilateral hexagons, which means that the grid type of the close-packed plane is 6^3. In the sub-outer layer, inter-distance of the Sm atoms is ~ 5.56 Å, and a 3^6 grid structure can be detected. In the central layer, as occupied by the Zn atoms, a 3636 grid can be found, which corresponds to the “equilateral triangle - equilateral hexagon - equilateral triangle - equilateral hexagon” structure. Inter-distance between the Zn atoms is ~ 2.78 Å. And the five-layer unit-cell, with three types of grid structures, forms a “6^3+3^6+3636+3^6+6^3” topologically close-packed structure with thickness of ~ 4.83 Å in the $_{a}$ direction. Finally, the chemical formula of the 2D Frank-Kasper *Z* precipitate can be determined to be $Mg_2Sm_2Zn_3$.

Simulated electron diffraction patterns of the new generated *Z*-$Mg_2Sm_2Zn_3$ model and the corresponding SAED patterns of the precipitate-plate in the *α*-Mg matrix are presented in the Supplemental Fig. S4. It can be found that the simulation results are well consistent with the experimental observations, further verified the validity of the structure we constructed.

Generally, the atomic clusters have a higher stacking density and a lower free energy of system [1, 2, 22]. Fig. 3d exhibits a 3D icosahedron cluster model in the *Z*-$Mg_2Sm_2Zn_3$ precipitate along the $_Z$ direction, and an atomic number of "…1-5-1-5-1…" chain structure can be observed, suggesting that the central atom (Zn atom-sphere) is in contact with 12 atom-spheres. Fig. 3e presents a 3D view of icositetrahedron chain structure model with an atomic number of "…1-6-1-6-1…", and the Sm atom-sphere is located at the central position. In this configuration, the top sphere (dotting blue sphere) is the adjacent to Mg atom in the matrix only then can form such a polyhedron with a *CN* of 14, since the 2D structure is confined in the $_Z$ direction. Unfortunately, what it needs to be pointed out is that the icositetrahedron with *CN* = 14 has not been observed yet in this system. However, Fig. 3f provides a novel 3D irregular polyhedron with a *CN* of 16 which is confirmed by experimental observations, and the top spheres (3 solid red spheres) are also adjacent to the matrix Mg atoms, and thus can generate such a chain structure with an atomic number of "3-6-1-6-1".

The results of first-principles calculations for the 2D Frank-Kasper *Z*-$Mg_2Sm_2Zn_3$ phase are provided in Fig. 4 and the Supplemental Table S3. An unrelaxed structure with a stacking sequence of "ACA", *i.e.*, the initial state of the precipitate-plate without considering lattice distortion and rearrangements of atoms, is shown in Fig. 4a. In which the atomic layer "A" is completely consistent with the matrix layer, and just some Mg positions are replaced orderly by the Sm atoms. The corresponding geometry relaxed structure is presented in Fig. 4b. Obviously, the optimized structure is different from the initial state, a simple atomic shuffling by self-adaption, can transform the monoatomic "A" layer to a double-layers structure (marked as "A‴") containing Mg and Sm atomic layer, achieving the transition from simpler crystal to the complex close-packed structure. In addition, the formation energy of the 2D *Z*-$Mg_2Sm_2Zn_3$ precipitate is 38.54 *meV*, meaning that such a structure cannot generated independently. Fig. 4c shows an optimized "ABA-A'CA'-AB" sandwiched model containing matrix Mg layers. The bonding of "A-A‴" layers means that the ideal icositetrahedrons with *CN* = 14 mentioned above in Fig. 3e are generated, however, this state is thermodynamically metastable, with a formation energy of only -18.79 *meV*. The experimentally observed sandwiched model with a stacking sequence of "BAB-A'CA'-BA" (in Fig. 2f) is also optimized, and presented in Fig. 4d. The connection of "B-A‴" layers then form the irregular polyhedron with a *CN* of 16 mentioned above in Fig. 3f. The formation energies of such a structure is -88.19 *meV*, indicating that this configuration is thermodynamically more stable. And lattice parameters (Fig. 4d) of the optimized structure are well consistent with the experimental measurements. Moreover, it is worth mentioning that traditional Frank-Kasper twenty-eighth polyhedron with *CN* = 16 is totally different from the irregular polyhedron determined here [23].

The charge distribution of the “BAB-A’CA’-BA” sandwiched model viewed along the *Z* direction is shown Fig. 4e. It can be found that there is a mass of electrons accumulated at the *Z*-$Mg_2Sm_2Zn_3$/*α*-Mg hetero-interface, and less charge distributed in the central Zn layer, indicating that the Mg and Sm atoms on the outermost layers bonding stronger. Additionally, the electron localized function results exhibited in Figs. 4f-i illustrates same conclusion as the charge distribution analysis, that is, obviously covalent characteristic bonding in the outermost layers, and weaker bonding in the central Zn layer.

The formation of Frank-Kasper *Z* phases is usually inhibited due to a relatively large volume ratio among the its constituents [9, 10, 24]. Since the first proposed of the Zr_4Al_3 phase by *C. G. Wilson et al* in 1960 based on X-ray diffraction results [16], the structure has not been confirmed by any other TEM experimental observations to date. However, we unambiguously confirmed here the existence of a 2D Frank-Kasper Z fundamental structure with only one unit-cell thickness in the crystallography. It should be noted that the validated 2D Frank-Kasper *Z* structure is a meta-stable phase, as evidenced by TEM analysis in Supplemental Fig. S5, and the *Z*-$Mg_2Sm_2Zn_3$ precipitate would generate more stacking faults with a prolonged ageing.

In conclusion, we have identified a new type of 2D Frank-Kasper *Z* phase precipitated in a model Mg-Sm-Zn ternary system. Based on the atomic-scale HAADF-STEM observations combined with DFT computations, the crystal structure, chemical composition, and the atomic coordinates of the Z precipitate-plate are fully unraveled. The confined *Z*-$Mg_2Sm_2Zn_3$ phase has an ordered hexagonal structure (space group: P6/mmm, a = 5.56 Å, c = 4.83 Å), and with one unit-cell height in the $_a$ direction. The 2D *Z*-$Mg_2Sm_2Zn_3$ phase has a stacking sequence of “…-AB-A’CA’-BA-…” along the $_a$ axis. A new structured Frank-Kasper cluster model with *CN* = 16 has been confirmed. This finding is interesting and important to understand the formation mechanism and clustering behavior of the Frank-Kasper phases, and a new class of 2D Frank-Kasper *Z* phases with $A_2B_2C_3$ in composition would be established in follow-up studies in the near future. It is also expected to provide a meaningful theoretical guidance for designing and developing novel high-strength alloys strengthened by the 2D Frank-Kasper *Z* precipitates.

Declarations

Acknowledgements

The authors acknowledge the National Key Research and Development Program of China (Grant No. 2016YFB0701202), the National Natural Science Foundation of China (Grant No. 51525101, No. 51971053, No. U1610253), the Fundamental Research Funds for the Central Universities (Grant No. N2002018), the Project of Promoting Talents in Liaoning Province (No. XLYC1808038), and the Project funded by China Postdoctoral Science Foundation (2020M670774). The authors extend their gratitude to Prof. Yonghui Sun and Dr. Yu Dong (Analytical and Testing Center, Northeastern University) for their help with the Cs-corrected HAADF-STEM technique.

References

1. Frank, F. C. & Kasper, J. S. Complex alloy structures regarded as sphere packings. I. Definitions and basic principles. Acta Crystallogr. 11, 184–190 (1958).
2. Frank, F. C. & Kasper, J. S. Complex alloy structures regarded as sphere packings. II. Analysis and classification of representative structures. Acta Crystallogr. 12, 483–499 (1959).
3. Xie, H. B. et al. New structured Laves phase in the Mg-In-Ca system with nontranslational symmetry and two unit cells. *Phys. Rev. Lett.* **120**, 085701 (2018).
4. Xie, H. B. et al. Self-assembly of two unit cells into a nanodomain structure containing five-fold symmetry. *J. Phys. Chem. Lett.* **9**, 4373–4378 (2018).
5. Vargas, R., Mariani, P., Gulik, A. & Luzzati, V. Cubic phases of lipid-containing systems: the structure of phase Q223 (space group Pm3n). An x-ray scattering study. *J. Mol. Biol.* **225**, 137–145 (1992).
6. Luzzati, V. et al. Lipid polymorphism: a correction. The structure of the cubic phase of extinction symbol Fdc- consists of two types of disjointed reverse micelles embedded in a three-dimensional hydrocarbon matrix. *Biochemistry* **31**, 279–285 (1992).
7. Hudson, S. D. et al. Direct visualization of individual cylindrical and spherical supramolecular dendrimers. *Science* **278**, 449–452 (1997).
8. Lee, S. Bluemle, M. J. & Bates, F. S. Discovery of a Frank-Kasper s phase in sphere-forming block copolymer melts. *Science* **30**, 349–353 (2010).
9. Kim, K. et al. Thermal processing of diblock copolymer melts mimics metallurgy. *Science* 356, 520–523 (2017).
10. Su, Z. B. et al. Identification of a Frank-Kasper Z phase from shape amphiphile self-assembly. *Nature Chem.* **11**, 899–905 (2019).
11. Keys, A. S. & Glotzer, S. C. How do quasicrystals grow? *Phys. Rev. Lett.* **99**, 235503 (2007).
12. Shechtman, D., Blech, I., Gratias, D. & Cahn, J. W. Metallic phase with long-range orientational order and no translational symmetry. *Phys. Rev. Lett.* **53**, 1951–1953 (1984).
13. Hajiw, S., Pansu, B. & Sadoc, J. F. Evidence for a C14 Frank_Kasper Phase in One-Size Gold Nanoparticle Superlattices. *ACS Nano* **9**, 8116–8121 (2015).
14. Yang, Q. B. & Kuo, K. H. A new description of pentagonal Frank-Kasper phases and a possible structure model of the icosahedral quasicrystal. *Acta Cryst.* **A43**, 787–795 (1987).
15. Wang, Z. M., Yang, Q. B. & Kuo, K. H. Description of hexagonal Frank-Kasper phases by a projection method. *Acta Cryst.* **A45**, 268–274 (1989).
16. Wilson, C. G., Thomas, D. K. & Spooner, F. J. The crystal structure of Zr_4Al_3. *Acta Cryst.* **13**, 56–57 (1960).
17. Nie, J. F. Precipitation and Hardening in Magnesium Alloys. *Metall. Mater. Trans.* **43A**, 3891–3939 (2012).

18. Nie, J. F. et al. Solute segregation and precipitation in a creep-resistant Mg-Gd-Zn alloy. *Acta Mater.* **56**, 6061–6076 (2008).
19. Xie, H. B. et al. Magnesium Alloys Strengthened by Nanosaucer Precipitates with Confined New Topologically Close-Packed Structure. *Cryst. Growth Des.* **18**, 5866–5873 (2018).
20. Kirkland, E. J., Loane, R. F. & Silcox, J. Simulation of annular dark field stem images using a modified multislice method. *Ultramicroscopy* **23**, 77–96 (1987).
21. Bos, K. H. et al. Unscrambling mixed elements using high angle annular dark field scanning transmission electron microscopy. *Phys. Rev. Lett.* **116**, 246101 (2016).
22. Kelton, K. F. Crystallization of liquids and glasses to quasicrystals. *J. Non-Cryst. Solids* **334**, 253–258 (2004).
23. Ye, H. Q., Li, D. X. & Guo, K. X. Topologically close-packed phases in superalloys: New phases and domain structures. *Acta Metal. Sin.* **22**, 1–43 (1986).
24. Reddy, A. et al. Stable Frank-Kasper phases of self-assembled, soft matter spheres. *Proc. Natl Acad. Sci. USA* **115**, 10233–10238 (2018).

Figures

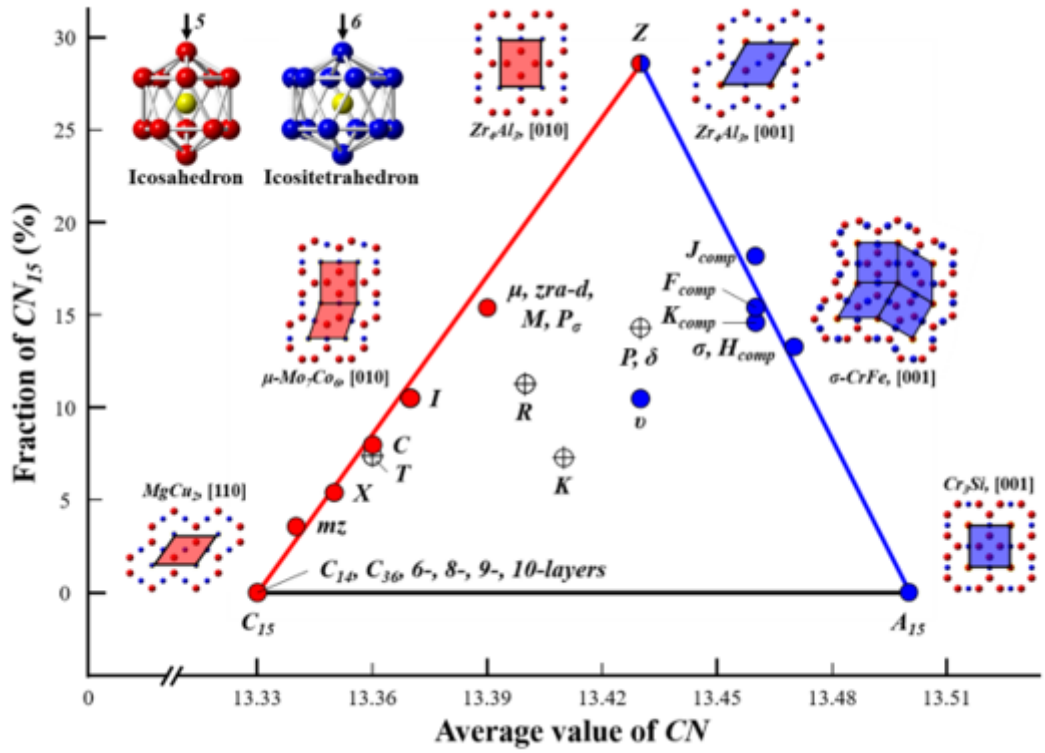

Figure 1

Frank-Kasper phases and polyhedra. The triangle includes all the Frank-Kasper phases experimentally observed so far, with C15, A15 and Z located at the three vertices of triangle. The horizontal axis is the

average CN and the vertical axis is the fraction of polyhedra with CN = 15. In which the pentagonal Frank-Kasper phases assembled by the C15 and Z plane tiling patterns are represented by the red color, and the hexagonal Frank-Kasper phases assembled by the A15 and Z plane tiling patterns are represented by the blue color. The corresponding models of icosahedron and icositetrahedron are presented in the top-left insets.

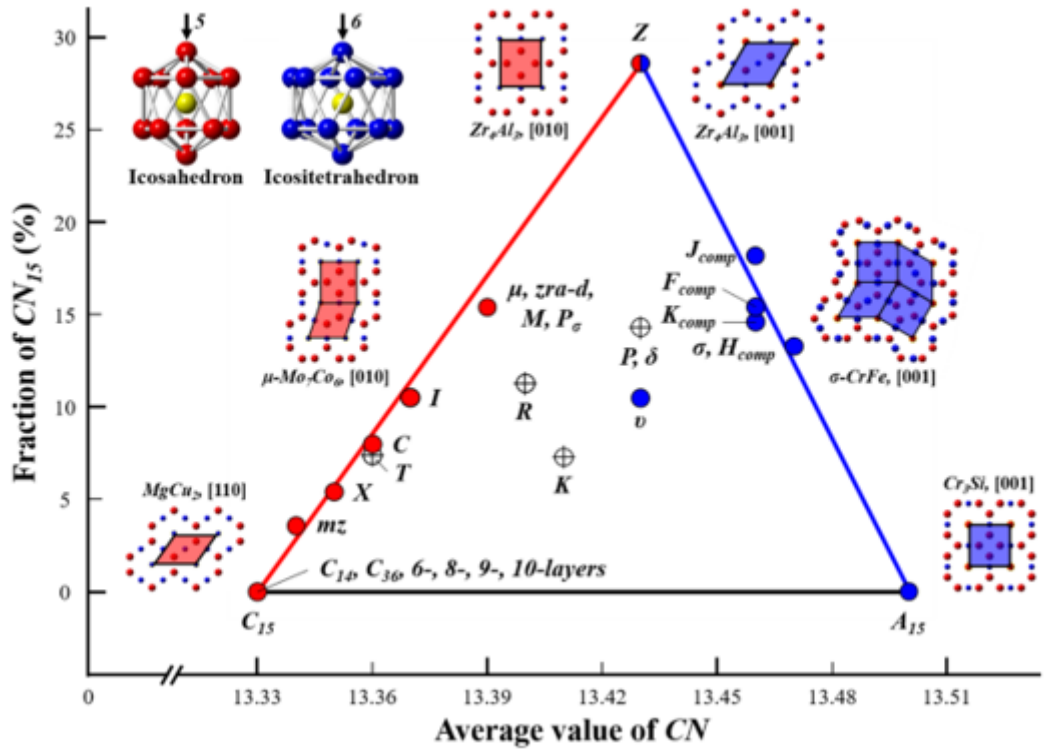

Figure 1

Frank-Kasper phases and polyhedra. The triangle includes all the Frank-Kasper phases experimentally observed so far, with C15, A15 and Z located at the three vertices of triangle. The horizontal axis is the average CN and the vertical axis is the fraction of polyhedra with CN = 15. In which the pentagonal Frank-Kasper phases assembled by the C15 and Z plane tiling patterns are represented by the red color, and the hexagonal Frank-Kasper phases assembled by the A15 and Z plane tiling patterns are represented by the blue color. The corresponding models of icosahedron and icositetrahedron are presented in the top-left insets.

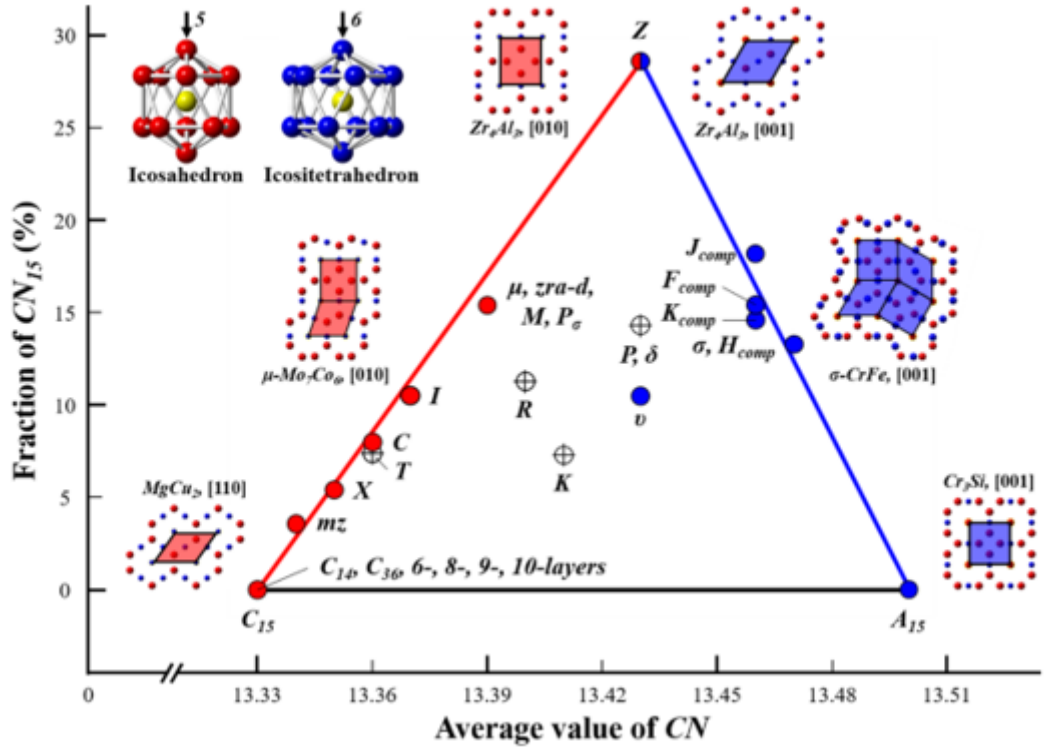

Figure 1

Frank-Kasper phases and polyhedra. The triangle includes all the Frank-Kasper phases experimentally observed so far, with C15, A15 and Z located at the three vertices of triangle. The horizontal axis is the average CN and the vertical axis is the fraction of polyhedra with CN = 15. In which the pentagonal Frank-Kasper phases assembled by the C15 and Z plane tiling patterns are represented by the red color, and the hexagonal Frank-Kasper phases assembled by the A15 and Z plane tiling patterns are represented by the blue color. The corresponding models of icosahedron and icositetrahedron are presented in the top-left insets.

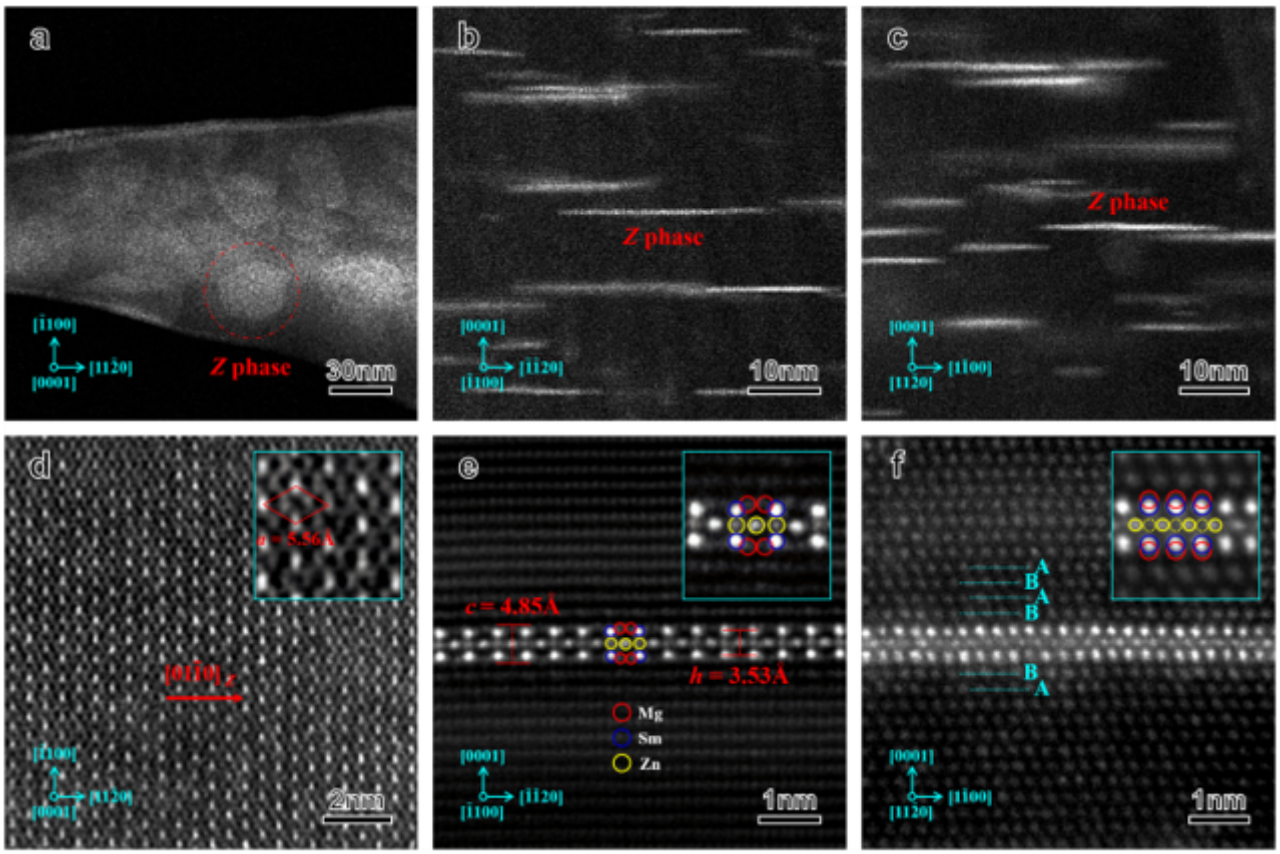

Figure 2

HAADF-STEM images of the 2D Frank-Kasper Z phase in a Mg-4Sm-2Zn (wt.%) alloy after aged at 200 °C for 48 h. These precipitates are obtained from three perpendicular zone axes of [0001]α (a and d), [1100]α (b and e), and [11$\bar{2}$0]α (c and f). The insets in Figs. 2d-f show the enlarged images of some local parts of the precipitates, and Mg atoms in outmost layers are marked with red circles, Zn (in sub-outer layers) and Sm (in center layer) atoms are marked with blue and yellow circles, respectively.

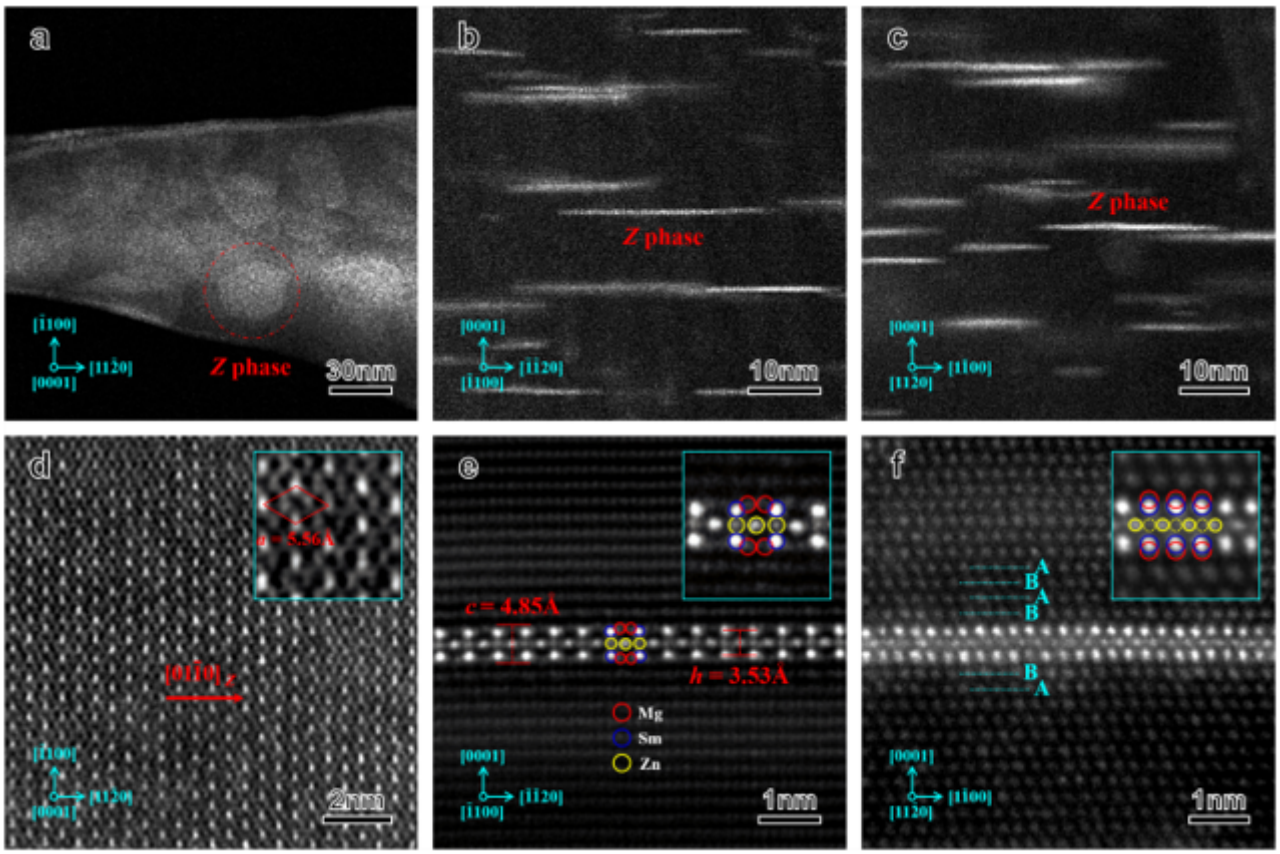

Figure 2

HAADF-STEM images of the 2D Frank-Kasper Z phase in a Mg-4Sm-2Zn (wt.%) alloy after aged at 200 ºC for 48 h. These precipitates are obtained from three perpendicular zone axes of [0001]α (a and d), [1100]α (b and e), and [11$\bar{2}$0]α (c and f). The insets in Figs. 2d-f show the enlarged images of some local parts of the precipitates, and Mg atoms in outmost layers are marked with red circles, Zn (in sub-outer layers) and Sm (in center layer) atoms are marked with blue and yellow circles, respectively.

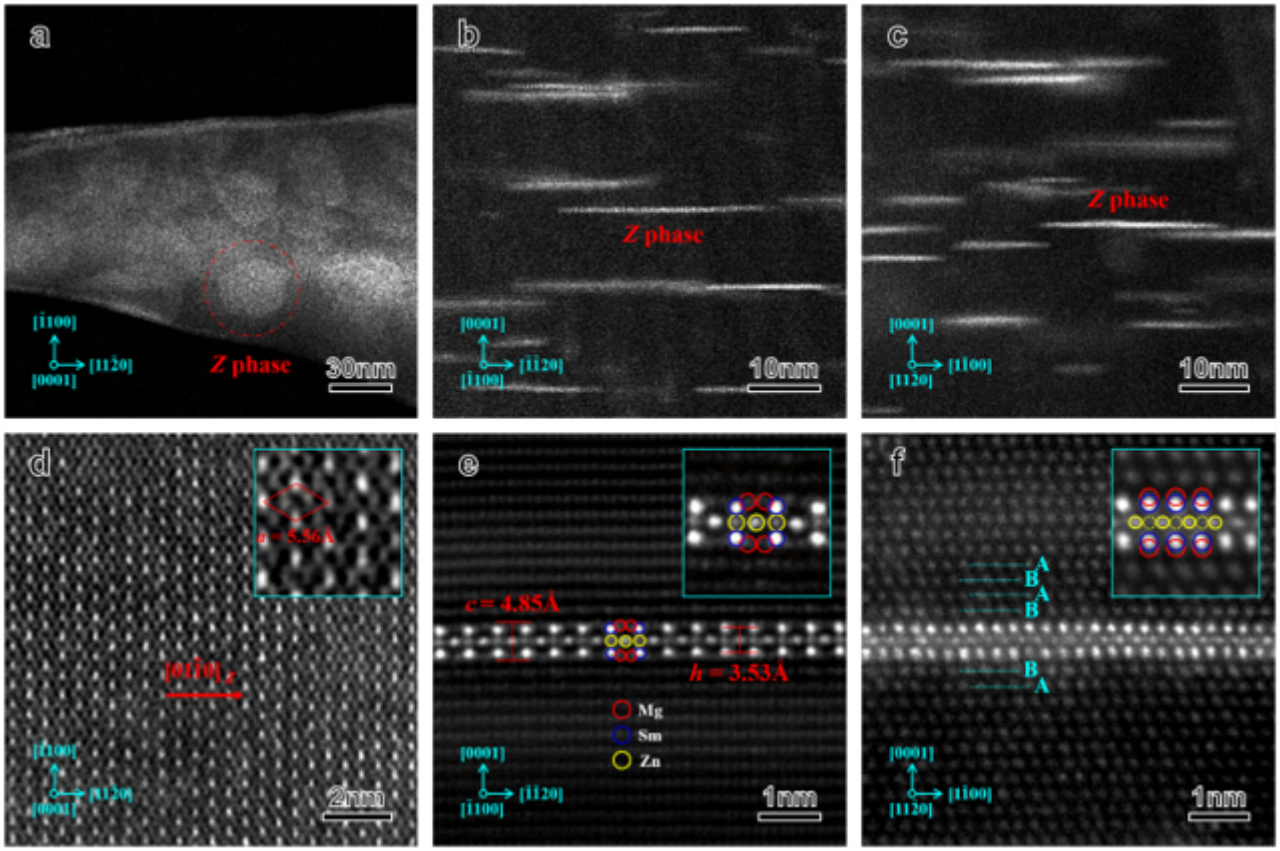

Figure 2

HAADF-STEM images of the 2D Frank-Kasper Z phase in a Mg-4Sm-2Zn (wt.%) alloy after aged at 200 °C for 48 h. These precipitates are obtained from three perpendicular zone axes of [0001]α (a and d), [1100]α (b and e), and [11$\bar{2}$0]α (c and f). The insets in Figs. 2d-f show the enlarged images of some local parts of the precipitates, and Mg atoms in outmost layers are marked with red circles, Zn (in sub-outer layers) and Sm (in center layer) atoms are marked with blue and yellow circles, respectively.

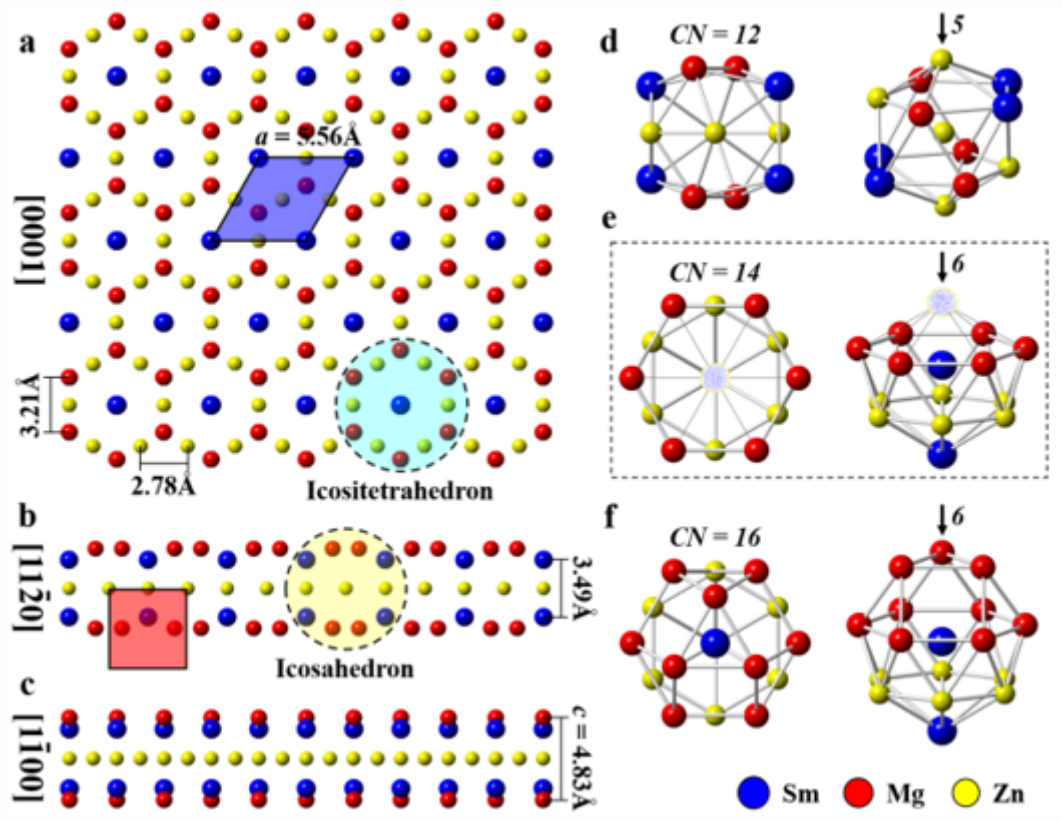

Figure 3

Modeled atomic arrangements and clusters of the 2D Frank-Kasper Z-Mg2Sm2Zn3 phase. The direction is viewed along the [0001]Z (a), [11$\bar{2}$0]Z (b), and [1$\bar{1}$00]Z (c), respectively. (d-f) Three-dimensional atomic cluster models: (d) Icosahedron, CN = 12; (e) Icositetrahedron, CN = 14; (f) Irregular polyhedron, CN = 16.

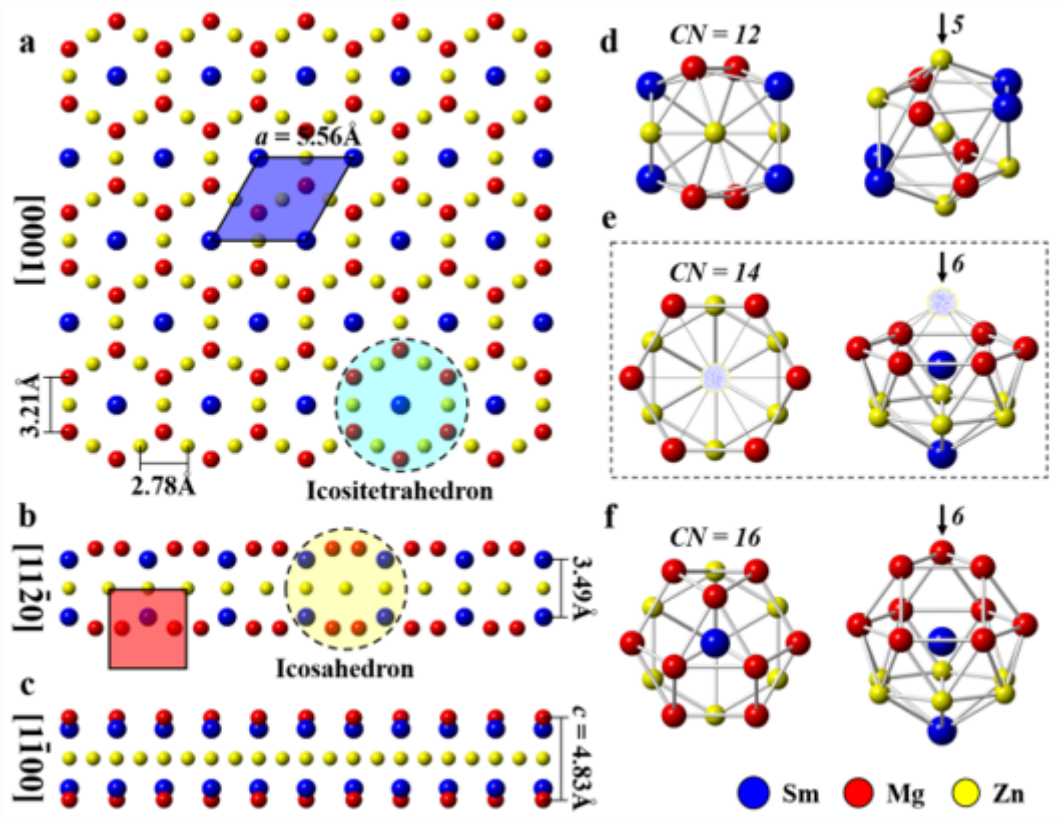

Figure 3

Modeled atomic arrangements and clusters of the 2D Frank-Kasper Z-Mg2Sm2Zn3 phase. The direction is viewed along the [0001]Z (a), [11$\bar{2}$0]Z (b), and [1$\bar{1}$00]Z (c), respectively. (d-f) Three-dimensional atomic cluster models: (d) Icosahedron, CN = 12; (e) Icositetrahedron, CN = 14; (f) Irregular polyhedron, CN = 16.

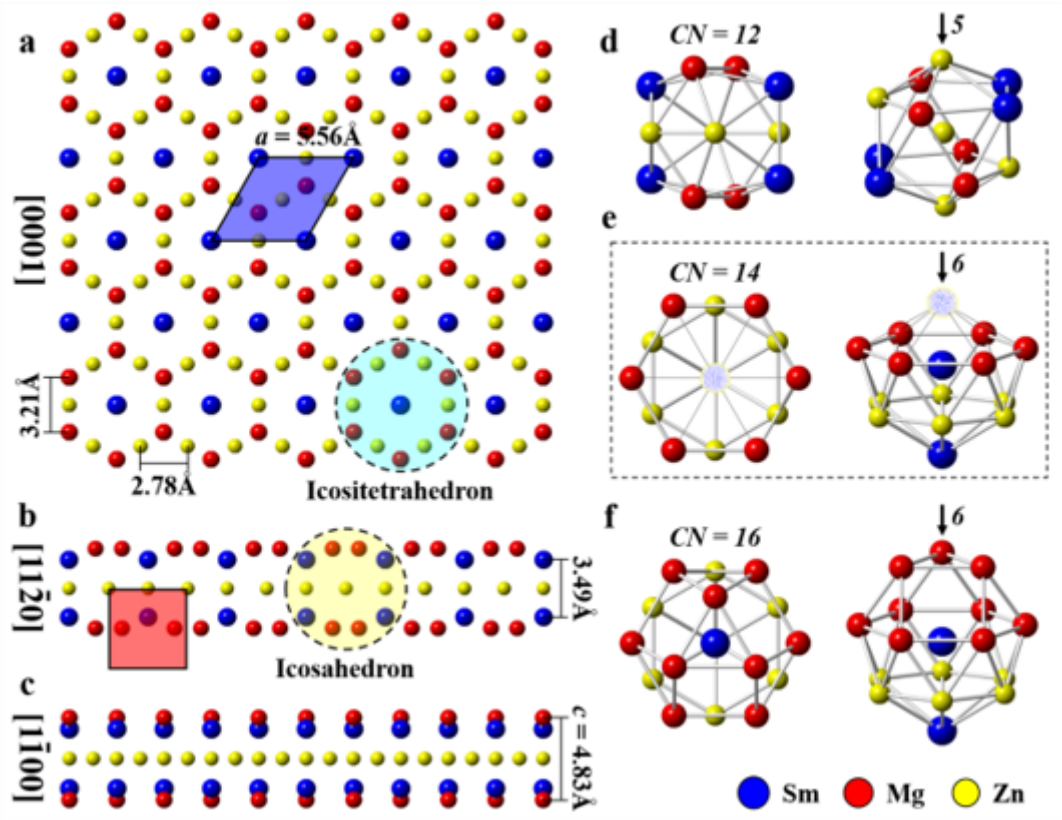

Figure 3

Modeled atomic arrangements and clusters of the 2D Frank-Kasper Z-Mg2Sm2Zn3 phase. The direction is viewed along the [0001]Z (a), [11$\bar{2}$0]Z (b), and [1$\bar{1}$00]Z (c), respectively. (d-f) Three-dimensional atomic cluster models: (d) Icosahedron, CN = 12; (e) Icositetrahedron, CN = 14; (f) Irregular polyhedron, CN = 16.

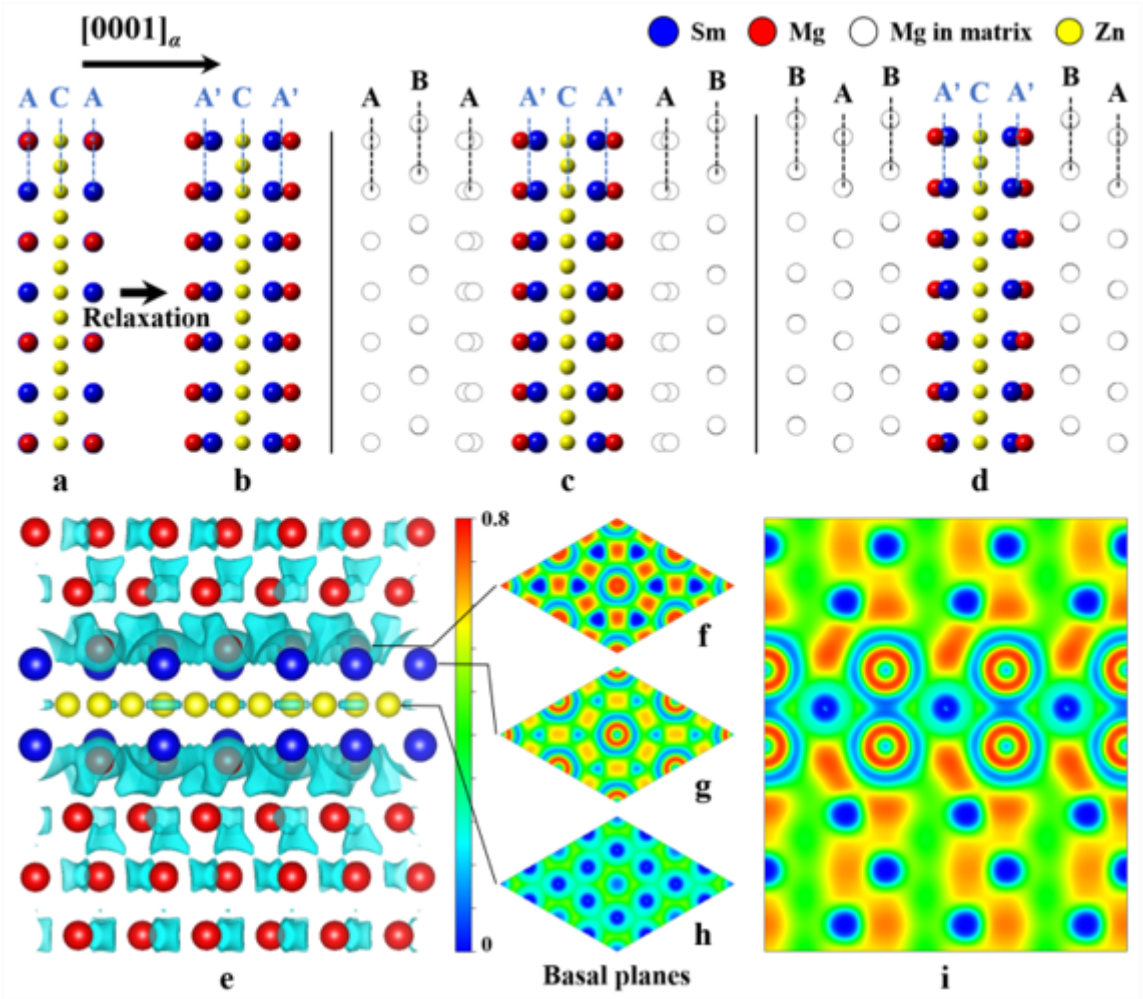

Figure 4

DFT computations results of the 2D Frank-Kasper Z-Mg2Sm2Zn3 phase. The direction is viewed along the [11¯00]Z (a-e, and i) and [0001]Z (f-h). (a and b) Atomic arrangements of the 2D Frank-Kasper Z-Mg2Sm2Zn3 phase at initial (a) and relaxed (b) states in the simulation processes. (c and d) The relaxed sandwiched models which containing the Z-Mg2Sm2Zn3 phase: (c) “ABA-A’CA’-AB” model; (d) “BAB-A’CA’-BA” model. (e) Charge distribution of the “BAB-A’CA’-BA” sandwiched model. (f-i) The corresponding electron localization function distribution for the slices of {0001}Z (f-h) and {11¯00}Z (i) sections. The charge iso-surface setting using the Δρ = 0.015 e·Å-3 in the panels.

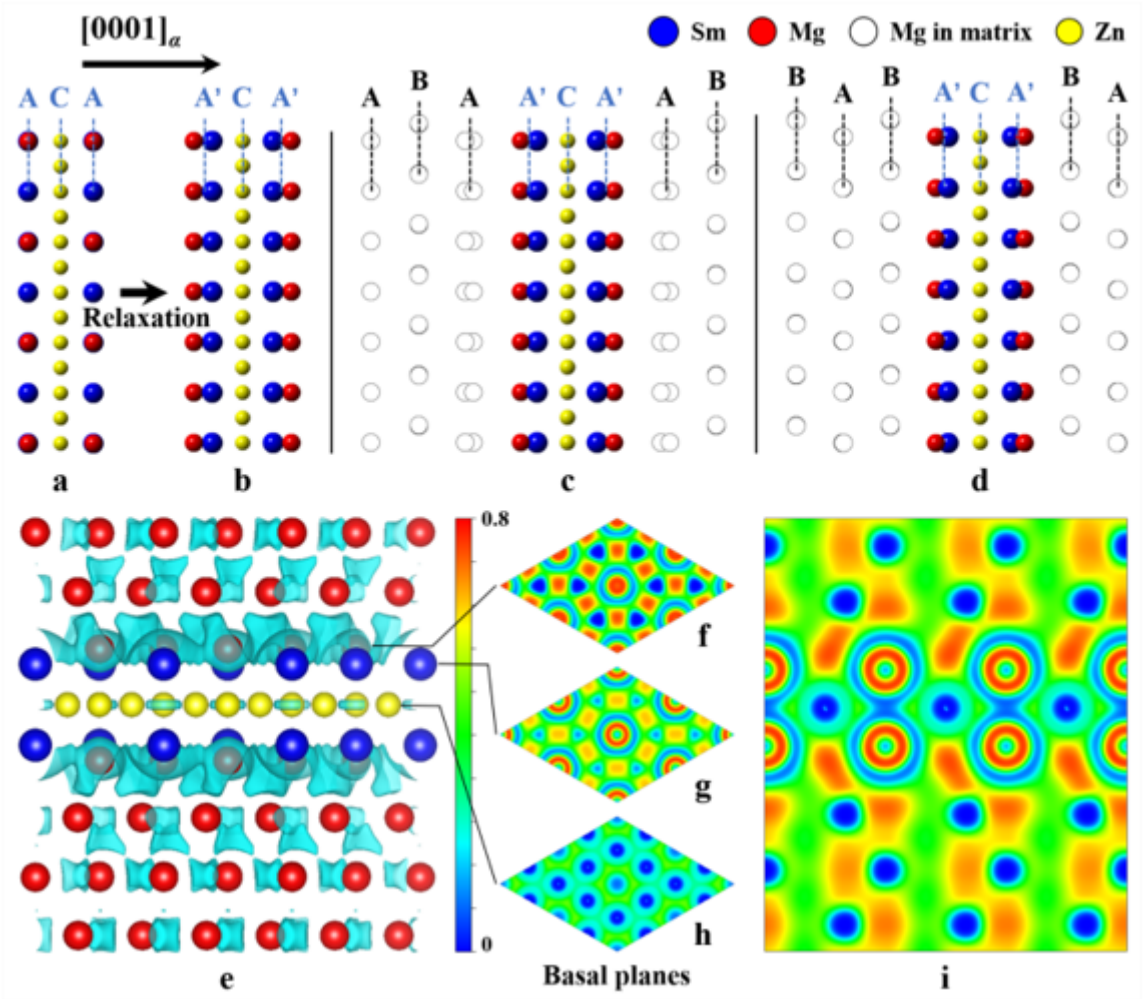

Figure 4

DFT computations results of the 2D Frank-Kasper Z-Mg2Sm2Zn3 phase. The direction is viewed along the [11¯00]Z (a-e, and i) and [0001]Z (f-h). (a and b) Atomic arrangements of the 2D Frank-Kasper Z-Mg2Sm2Zn3 phase at initial (a) and relaxed (b) states in the simulation processes. (c and d) The relaxed sandwiched models which containing the Z-Mg2Sm2Zn3 phase: (c) “ABA-A’CA’-AB” model; (d) “BAB-A’CA’-BA” model. (e) Charge distribution of the “BAB-A’CA’-BA” sandwiched model. (f-i) The corresponding electron localization function distribution for the slices of {0001}Z (f-h) and {11¯00}Z (i) sections. The charge iso-surface setting using the Δρ = 0.015 e·Å-3 in the panels.

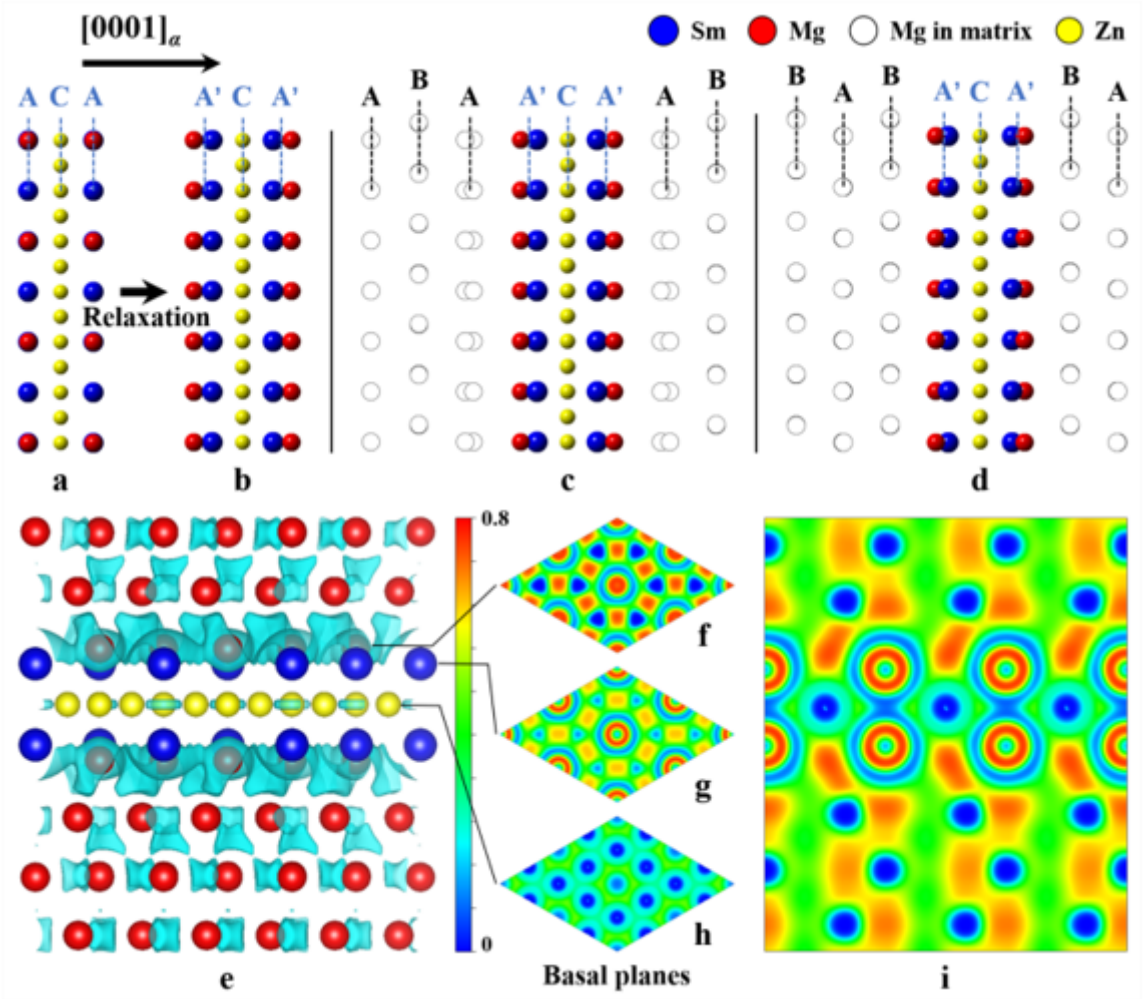

Figure 4

DFT computations results of the 2D Frank-Kasper Z-Mg2Sm2Zn3 phase. The direction is viewed along the [11¯00]Z (a-e, and i) and [0001]Z (f-h). (a and b) Atomic arrangements of the 2D Frank-Kasper Z-Mg2Sm2Zn3 phase at initial (a) and relaxed (b) states in the simulation processes. (c and d) The relaxed sandwiched models which containing the Z-Mg2Sm2Zn3 phase: (c) “ABA-A’CA’-AB” model; (d) “BAB-A’CA’-BA” model. (e) Charge distribution of the “BAB-A’CA’-BA” sandwiched model. (f-i) The corresponding electron localization function distribution for the slices of {0001}Z (f-h) and {11¯00}Z (i) sections. The charge iso-surface setting using the Δρ = 0.015 e·Å-3 in the panels.

Supplementary Files

This is a list of supplementary files associated with this preprint. Click to download.

- SupplementaryMaterials.docx
- SupplementaryMaterials.docx
- SupplementaryMaterials.docx